The International Journal of Advanced Manufacturing Technology (2020) 108:2607–2619
https://doi.org/10.1007/s00170-020-05439-y

ORIGINAL ARTICLE

Characteristics of shear stress based on magnetorheological fluid flexible fixture during milling of the thin-walled part

Jiang Xiaohui[1] · Zhang Yong[1] · Lu Weiwei[1] · Gao Shan[1] · Liu Ling[2] · Liu Xiao[3]

Received: 28 December 2019 / Accepted: 8 May 2020 / Published online: 12 June 2020

Abstract
With light weight and good overall structure, thin-walled part has been widely used in various fields like aerospace. However, it has low stiffness in the cutting process. Traditional fixture clamping workpiece has a long positioning and adjustment cycle and is likely to deform, making it difficult to control machining efficiency and quality. In this study, a mechanical-magnetorheological fluid (MRF) composite flexible clamping method was proposed, and a theoretical mathematical model of the shear stress of MRF was constructed. The real value and the theoretical value of shear stress show consistent upward and downward trends. Based on the prediction model, the coupling relations between magnetic field intensity and thickness and position of workpiece were studied. Results demonstrate that workpiece thickness has less significant influence on shear stress compared with workpiece position. Combined with the experimental results, the smaller the workpiece thickness and the closer to the magnetic field, the larger the shear stress. The shear stress of the workpiece 1 mm thick is 21.5% higher than that of the workpiece with the thickness of 8 mm at position of 10 mm. Finally, the thin-walled part was used to demonstrate MRF clamping. Compared with the traditional clamping method, the proposed method can decrease the cutting force by 14.3%. Moreover, the residual stress σ_x and σ_y decrease by 37.0% and 43.9%, the flatness value decreases by 55.6%, and the roughness R_a, R_z and R_q decrease by 55.6%, 53.2%, and 56.7%. The quality of the thin-walled part was effectively controlled.

Keywords Thin-walled part · MRF flexible fixture · Shear stress · Workpiece position · Workpiece thickness

1 Introduction

Thin-walled parts, characterized by small thickness, low structural stiffness, irregular shape, and high material removal rate, are the key components of high-end equipment in aerospace and automobile field [1]. Currently, thin-walled parts are mostly shaped by milling machine tools. However, rigid contact area between traditional fixture and workpiece is small. Uneven force of parts leads to processing deformation and poor surface quality. Therefore, studying the machining and clamping performance of flexible fixture is of great significance to improve the surface quality of parts.

Previous methods improved the surface quality of parts from two aspects: process parameter optimization and path algorithm optimization [2, 3]. Cep et al. [4] processed the workpiece by only changing feed rate while keeping other cutting parameters unchanged, finding that decreasing feed rate can improve the surface roughness of workpieces to some extent. In order to enhance the milling stability and improve the surface quality, Dong et al. [5] proposed a milling dynamic model which transformed a dynamic model with a small discrete interval and multiple variables into a state equation, which was integrated into a manufacturing system multivariable in the range of the milling depth. Based on genetic algorithm, Savadamuthu et al. [6] proposed an optimization model to optimize the processing parameters of turning process, which significantly improved the processing efficiency considering the constraints of technology and materials. Hareendran et al. [7] carried out a series of machining experiments and used surface photometer and data statistical software to tabulate the roughness value of different samples

✉ Jiang Xiaohui
jiangxh@usst.edu.cn

[1] College of Mechanical Engineering, University of Shanghai for Science and Technology, Shanghai 200093, China

[2] School of Mechanical and Electronical Engineering, Lanzhou University of Technology, Lanzhou 730050, China

[3] Shanghai Aerospace Equipment Manufacturing Company Limited, Shanghai, China

under various cutting conditions. They found that tool parameters are the main factors influencing the surface quality of the workpiece, and the interaction of the machining parameters can decrease the machining accuracy. Based on the results, they proposed the method of controlling tool geometric tolerance and drew the conclusions. Combining two approaches of artificial intelligence (artificial neural networks and genetic algorithms), Kant et al. [8] and Ding et al. [9] developed a prediction and optimization model which can replace the conventional method to predict the optimal processing parameters and optimize the surface quality. An artificial neural network was proposed to predict cutting forces by Tandon et al. [10]. Particle swarm optimization was employed to effectively optimize machining parameters of milling and improve the surface quality of parts. Hauth et al. [11] put forward a constant scallop height tool path generation method, which has been widely used in the industrial field. Rao et al. [12] explored the application of the nontraditional optimization method in the optimization of milling parameters with multiple feed, significantly improved the surface quality of parts. Jiang et al. [13–15] used the AdvantEdge cutting simulation software and experiments to study the effects of milling parameters and tool diameter on cutting force and residual stress of workpiece, finding that the milling efficiency and surface quality of workpiece can be guaranteed by appropriately increasing milling speed and matching small cutting depth. Wu et al. [16] investigated the high-speed grinding to reveal the application of high-speed grinding technique in precision machining of the workpiece. The above methods for ameliorating surface quality are based on changing process parameters, optimizing path algorithm. However, the machining error caused by the point contact between fixture and workpiece is not fundamentally improved.

In addition to the above process parameters and path algorithm, milling clamping layout, clamping force, and workpiece-fixture contact behavior are also the key factor which can affect the machining quality. Xiong et al. [17] proposed a general method to determine the optimal clamping force, including the size and location of the clamping force. Deng et al. [18] used coupling dynamic models, such as machining dynamic model, geometric model, and static model, to guarantee the dynamic stability of machining with minimum clamping forces and analyzed the influence of material removal rate on system stability. With the maximum deformation of the workpiece as the objective function, Kaya et al. [19] used genetic algorithm to optimize the clamping layout and force and established a finite element evaluation model considering dynamic cutting load. In [20–22], the finite element method was employed to obtain the milling force of thin-walled parts and displacement of the workpiece in the cutting process, and the contact stiffness of fixture-workpiece was calculated. However, the method failed to optimize the fixture layout. In [23], Qin et al. established a clamping constraint model considering clamping force and sequence, and calculated the contact force and deformation during the clamping process according to the minimum residual energy principle. Liu et al. [24] investigated the finite element method to repeatedly calculate the maximum deformation region of the part and arrange fixture components in the region. Moreover, genetic algorithm was used to optimize the layout of the fixture components. However, they ignored the effect of dynamic load on the fixture layout. Raghu et al. [25] modeled the loading and clamping process of parts and used isomechanics to achieve the whole stiffness of the fixture-workpiece system. Also, the contact deformation at the contact point of the workpiece and the fixture was solved. Meshreki et al. [26–28] divided the frame structure into plate and spring models, and used the genetic algorithm and finite element software to calibrate the spring as the boundary condition. The plate model was replaced with Euler-Bernoulli beam dynamic model to optimize support layout of the fixture. Wan et al. [29] proposed a workpiece positioning scheme driven by machining features, which was employed to constrain the degree of freedom of workpiece with various machining features. They proposed a criterion for evaluating the effect of the positioning scheme. The above studies enhanced the clamping layout and force, but there were still some deficiencies, such as small contact area, uneven clamping force, and poor clamping performance.

As for the application of magnetorheological fluid, Zhang et al. [30] invented a clamping device for magnetorheological fluid workpiece as early as 2001. When the workpiece was placed in the magnetorheological fluid, the magnetorheological fluid was first solidified under the action of external magnetic field and then pressurized along the direction of magnetic field, thus obtaining greater clamping force. However, the device only applies to the machining of small irregular parts. Choi et al. [31] designed an instrument based on a hybrid magnetorheological damper, which was applied to the vibration control of flexible beams, and found that the vibration of flexible beams could be well suppressed by appropriate methods. Pour et al. [32] introduced an integrated mechatronic model for the chatter analysis of a machine tool equipped with MR damper, and the stiffness and damping of the machine tool were changed semi-actively by means of a MR damper to suppress chatter. The above devices based on MR fluid are still in the shallow layer, and their application in the milling of machine tools to study the clamping performance of fixtures and improve the quality of the workpiece has not been deeply explored.

In this study, conventional fixture was replaced with the magnetorheological fluid flexible fixture to fix the workpiece on the machine tool for milling. First of all, traditional fixture takes much time to clamp workpiece and is likely to deform, making it hard to control machining quality. Second, point contact exists between traditional fixture and workpiece; uneven force of parts leads to processing deformation and poor

surface quality. However, using magnetorheological fluid flexible fixture to fix the workpiece can totally cover parts and make the force uniform, suitable for any shape of irregular parts. Based on the combination of theory and experiment, the shear stress performance of flexible magnetorheological fluid fixture was investigated, and different thickness and position of workpiece were utilized to obtain the fixture scheme with the best clamping performance, thus finding the optimal solution of shear stress.

2 Methodology

This study investigated the relations between shear stress of MRF flexible fixture and the thickness and position of the workpiece using theoretical methods to determine the optimal machining position for workpiece. Moreover, experiments were carried out to demonstrate its reliability. Firstly, the mathematical model of MR fluid shear stress was carried out based on theoretical analysis, and reasonable hypothesis was made. By measuring magnetic field intensity, workpiece thickness, and workpiece position, the calculation formula of field intensity was fitted and substituted into the mathematical model. Second, the mathematical formula of actual shear stress was deduced by the friction coefficient experiment of shear stress, and the experimental data of shear stress was compared with the theoretical values. Finally, the accuracy of the conjecture was verified by the actual machining results.

2.1 Mathematical model of the MR fluid shear stress

The most important feature of MRF is shear stress, which represents its solidification intensity. Magnetic particles are magnetized under the action of magnetic field, and magnetic particles form a chain structure along the direction of the external magnetic field because of the magnetic force. In this section, the microscopic mathematical model of magnetic particles, under the action of magnetic field, is established from the microstructure of MRF, and the shear stress of MRF is calculated. Under the action of magnetic field, the magnetized particles produce the magnetic dipole moment. m_1 and m_2 are the moments of the two magnetic dipoles, and the magnetic interaction energy between the magnetic dipoles with distance of r is expressed as Eq. 1 [33]:

$$E = \frac{1}{4\pi\mu_0\mu_f}\left(\frac{\overrightarrow{m_1}\cdot\overrightarrow{m_2}}{r^3} - \frac{3\overrightarrow{m_1}\cdot\overrightarrow{m_2}\cdot\overrightarrow{r}^2}{r^5}\right) \tag{1}$$

where μ_0 is the permeability of vacuum, μ_f is the permeability of carrier fluid in MR fluids, and for magnetic particles, the value of the permeability of carrier fluid in MR fluids is about 1.

The chains are assumed to be arranged in parallel with equal spacing, and the interval is D_0. d_0 is the distance of the particles in the same chain, and R is the size. As shown in Fig. 1, after the shear deformation of MRF, the chain offset angle is θ. The magnetic dipole moment of the particles is equal, denoted as m, and the direction is in line with the magnetic field. The magnetic interaction energy is obtained.

$$E = \frac{m^2}{4\pi\mu_0\mu_f}\left(\frac{1-3\cos^2\theta}{r^3}\right) \tag{2}$$

According to the solidification characteristics of MR fluids, the direction of the chain is the same as the magnetic field. As shown in Fig. 2, a three-dimensional coordinate system is established by taking any particle in MR fluids as the coordinate origin. The particle coordinate from the origin at any position is set as (X, Y, Z). Suppose that the magnetic field is along the Z-direction, the shear occurs in the X-direction, and the particle displacement is in the X-direction, which is denoted as u. Therefore, the shear strain $\gamma = \tan\theta = \frac{u}{z}$, and displacement u can be expressed as below:

$$u = z\gamma \tag{3}$$

The new coordinate of the particle after shear deformation is $(x + z\gamma, y, z)$, and its distance from the origin of coordinate is defined as

$$r = \sqrt{(x+z\gamma)^2 + y^2 + z^2} \tag{4}$$

At the same time

$$\cos^2\theta = \frac{z^2}{(x+z\gamma)^2 + y^2 + z^2} \tag{5}$$

By substituting Eqs. 4 and 5 into Eq. 2, the magnetic interaction energy E can be obtained as

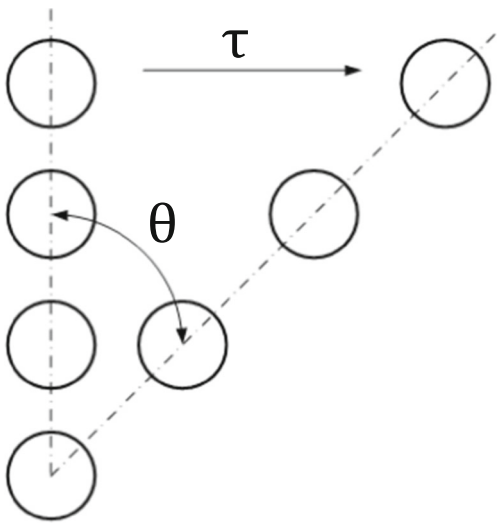

Fig. 1 Chain offset angle θ

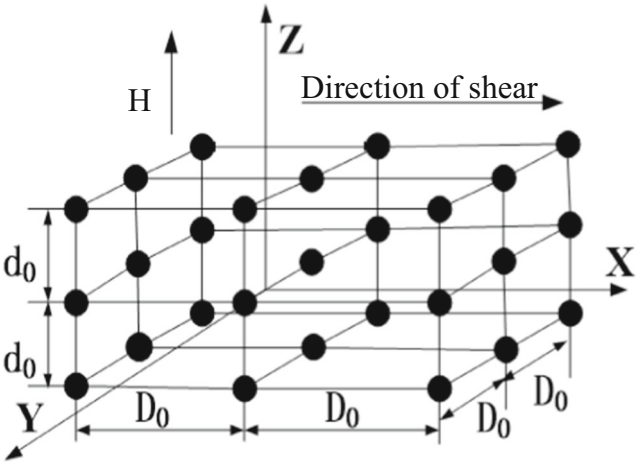

Fig. 2 Particle coordinate system

$$E = \frac{m^2}{4\pi\mu_0\mu_f}\frac{1-\dfrac{3z^2}{(x+z\gamma)^2+y^2+z^2}}{\left[(x+z\gamma)^2+y^2+z^2\right]^{\frac{3}{2}}} = \frac{\mathrm{m}^2}{4\pi\mu_0\mu_f}\frac{(\mathrm{x}+\mathrm{z}\gamma)^2+\mathrm{y}^2-2\mathrm{z}^2}{\left[(\mathrm{x}+\mathrm{z}\gamma)^2+\mathrm{y}^2+\mathrm{z}^2\right]^{\frac{5}{2}}} \tag{6}$$

The magnetic interaction energy exists between the particle at the coordinate origin and the particles everywhere in the space. Hence, the total magnetic interaction energy of the particle at the coordinate origin can be achieved by the sum of Eq. 6.

$$E_{\text{total}} = \sum\frac{m^2}{4\pi\mu_0\mu_{\mathrm{f}}}\frac{(x+z\gamma)^2+y^2-2z^2}{\left[(x+z\gamma)^2+y^2+z^2\right]^{5/2}} \tag{7}$$

The magnetic energy density of the MR fluid with volume V and concentration φ is written as follows:

$$E_{\mathrm{d}} = \frac{\frac{\varphi V/2}{4\pi R^3/3}E_{\text{total}}}{V} = \frac{3\varphi V E_{\text{total}}}{8\pi R^3 V} = \frac{3\varphi E_{\text{total}}}{8\pi R^3} = \frac{3m^2\varphi}{32\pi^2\mu_0\mu_f R^3}\sum\frac{(x+z\gamma)^2+y^2-2z^2}{\left[(x+z\gamma)^2+y^2+z^2\right]^{\frac{5}{2}}} \tag{8}$$

By calculating the partial derivative of the shear strain γ in Eq. 8, the shear stress under the action of magnetic field can be represented as Eq. 9:

$$\tau = \frac{\partial E_{\mathrm{d}}}{\partial\gamma} = \frac{9m^2\varphi}{32\pi^2\mu_0\mu_f R^3}\sum\frac{z(x+z\gamma)\left[4z^2-(x+z\gamma)^2-y^2\right]}{\left[(x+z\gamma)^2+y^2+z^2\right]^{7/2}} \tag{9}$$

The chains are parallel and evenly spaced in X and Y-directions, and the interval among the particles in the chains is equal. Assume that $x = kD_0$, $y = lD_0$, and $z = nd_0$, where k, l, and n are integers. The ratio of the chain spacing to the distance between adjacent particles in a chain is expressed as $\lambda = \frac{D_0}{d_0}$, so Eq. 9 can be rewritten as

$$\tau = \frac{9m^2\varphi}{32\pi^2\mu_0\mu_{\mathrm{f}}R^3}\sum\frac{nd_0(kD_0+\gamma nd_0)\left[4n^2d_0^2-(kD_0+\gamma nd_0)^2-l^2D_0^2\right]}{\left[(kD_0+\gamma nd_0)^2+l^2D_0^2+n^2d_0^2\right]^{7/2}} = \frac{9m^2\varphi}{32\pi^2\mu_0\mu_{\mathrm{f}}d_0^3R^3}\sum_{-k_{\max}}^{k_{\max}}\sum_{-l_{\max}}^{l_{\max}}\sum_{-n_{\max}}^{n_{\max}}\frac{n(k\lambda+\gamma n)\left[4n^2-(k\lambda+\gamma n)^2-l^2\lambda^2\right]}{\left[(k\lambda+\gamma n)^2+l^2\lambda^2+n^2\right]^{7/2}} \tag{10}$$

According to the single-chain dipole theory model, without considering the influence of surrounding chains, the shear stress of MR fluids is defined as [30]

$$\tau' = \frac{9m^2\varphi\Delta\gamma}{4\pi^2\mu_0\mu_{\mathrm{f}}d_0^3R^3} \tag{11}$$

where $\Delta = \sum_{n=1}^{\infty}\frac{1}{n^3}\approx 1.202$, $m = \left|\vec{m}\right| = 3\mu_{\mathrm{f}}\mu_0\beta VH$, $V = 4\pi R^3/3$. $\beta = (\mu_{\mathrm{p}}-\mu_{\mathrm{f}})/(\mu_{\mathrm{p}}+2\mu_{\mathrm{f}})$. For magnetic particles, $\mu_{\mathrm{p}}\approx 10^3$, and the value of μ_{f} of carrier fluid is about 1 in MR fluids, so $\beta\approx 1$. μ_{p} and μ_{f} represent the relative permeability of particles and carrier fluid, and R is the particle radius.

The ratio of Eqs. 10 and 11 is α

$$\alpha = \frac{\tau}{\tau'} = \frac{1}{8\Delta\gamma}\sum_{-k_{\max}}^{k_{\max}}\sum_{-l_{\max}}^{l_{\max}}\sum_{-n_{\max}}^{n_{\max}}\frac{n(k\lambda+\gamma n)\left[4n^2-(k\lambda+\gamma n)^2-l^2\lambda^2\right]}{\left[(k\lambda+\gamma n)^2+l^2\lambda^2+n^2\right]^{7/2}} \tag{12}$$

As shown in Fig. 3, take a small unit containing a magnetic particle in the chain, which is assumed to be a cuboid, and the length, width, and height of the unit are D_0, D_0, and d_0, respectively. Suppose that $d_0 = aR$, and the relation between particle concentration and volume of the unit is expressed as Eq. 13

$$\varphi = \frac{4\pi R^3/3}{D_0^2d_0} = \frac{4\pi}{3\lambda^2a^3} \tag{13}$$

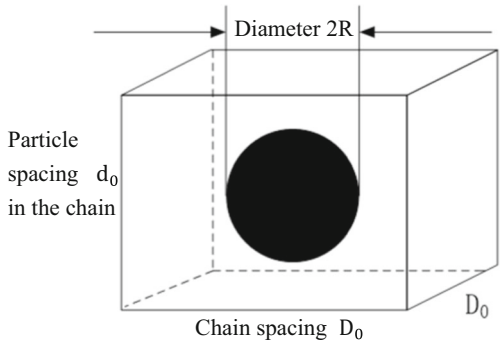

Fig. 3 Schematic cell

Therefore, Eq. 13 can be replaced by Eq. 14

$$\lambda = \left(\frac{4\pi}{3\varphi a^3}\right)^{1/2} \tag{14}$$

In the experiment, the permanent magnets are taken as the magnetic current source. To simplify the calculation, the approximate values of $k_{\max}$, $l_{\max}$, and $n_{\max}$ are 300, 300, and 1000. The MR fluid is mainly employed in the finishing of machine tools. Because the milling force is small, for the small strain case, assume that the shear strain $\gamma = 0.001$. Assume that $\lambda = 3$ and the dimensionless shear stress-strain relation caused by a constant magnetic field can be known from Eqs. 11 and 12, as shown in Fig. 4. When $\gamma = 0.37$, the shear stress of the MR fluid reaches the maximum value. Therefore, 0.37 is taken as the shear yield stress of MRF.

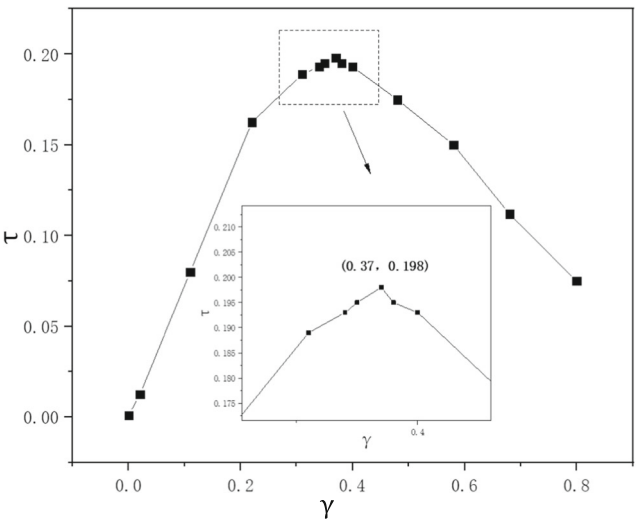

Fig. 4 Stress-strain dimensionless diagram

$$\tau|_{\gamma=0.37} = \frac{9m^2\varphi}{32\pi^2\mu_0\mu_f d_0^3 R^3} \sum_{-k_{\max}}^{k_{\max}} \sum_{-l_{\max}}^{l_{\max}} \sum_{-n_{\max}}^{n_{\max}} \frac{n(k\lambda+0.37n)\left[4n^2-(k\lambda+0.37n)^2-l^2\lambda^2\right]}{\left[(k\lambda+0.37n)^2+l^2\lambda^2+n^2\right]^{7/2}} \tag{15}$$

where $\varphi \approx 0.4$,R ≈ 5, $m = 16\pi^2 \times 10^{-7} \times R^3 \times H$. Without considering the repulsive force among magnetic particles in the chain, assume that $a = 2$, and $d_0 = 2R = 10$. $\lambda \approx 1.144$, $D_0 = 11.44$ can be obtained by Eq. 14, which are substituted into Eq. 15

$$\tau|_{\gamma=0.37} = 0.9\pi \times 10^{-7} H^2 \sum_{-k_{max}}^{k_{max}} \sum_{-l_{\max}}^{l_{\max}} \sum_{-n_{\max}}^{n_{\max}} \frac{n(1.144k+0.37n)\left[4n^2-(1.144k+0.37n)^2-l^2 1.144^2\right]}{\left[(1.144k+0.37n)^2+l^2 1.144^2+n^2\right]^{7/2}} \tag{16}$$

2.2 The relations between the thickness and position of workpiece and magnetic intensity

Equation 16 shows the correlation between shear stress and magnetic field intensity. However, in actual machining, the thickness and position of the part in the container can also affect the magnitude of magnetic field to which the workpiece is subjected. This section mainly carried on the experimental measurements on the above three relations and deduced the mathematical formula, which was introduced into Eq. 16 to obtain the relations between the shear stress and the thickness and position of workpiece.

The steps of the experiment are as follows: as shown in Fig. 5, the size of the container is 200 mm× 50 mm × 50 mm. The left container wall was taken as the starting position, and the container was divided into five parts equally. The corresponding location coordinates are 10 mm, 55 mm, 100 mm, 145 mm, and 190 mm. The workpieces are aluminum alloy thin-walled plates, and the thicknesses of the workpiece are 1 mm, 2 mm, 4 mm, 6 mm, and 8 mm, respectively. In the experiment on

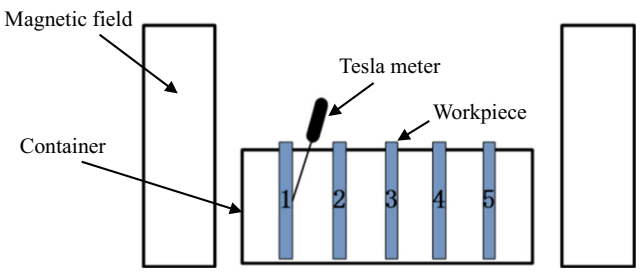

Fig. 5 Schematic diagram of experimental measurement with magnetic field intensity

magnetic field intensity, the MR fluid was not added in the container, and the magnetic field intensity of the left and right sides of the parts with different thicknesses was measured at different positions. The side close to the magnetic field is called the near magnetic field, and the opposite side is the far magnetic field, the average value of which is the average magnetic field. According to the measured data, the formula of the relations between the magnetic field and the thickness and position of the workpiece was fitted.

2.3 Experimental measurement of shear stress with magnetorheological fixture

Based on a series of assumptions in Section 2.2, the calculation formula of shear stress is obtained. However, it ignores the repulsive force between particles, the force between molecules, the friction force among MR fluids particles and containers, and workpiece. Furthermore, the magnetic particles are in a state of complete saturation, leading to a certain deviation from the actual processing. Therefore, in this section, the shear stress measurement experiment is designed in accordance with the experimental processing, and the actual shear stress formula is derived from the experimental data.

Figure 6 is a schematic diagram of the shear stress test. The test part is an aluminum alloy thin-walled plate with the size of 50 mm × 50 mm × 1 mm, and its attributes are the same as Section 2.2. The part was vertically submerged into the MR fluid with permanent magnets placed on both sides. The four walls of the part were subjected to the shear force F of the solidified MR fluid under the magnetic field, the friction f, and the gravity G of the workpiece. The measuring procedures are as follows: a dynamometer was used to slowly apply an upward pulling force F_{pull} on the measured part. As soon as the part showed the trend of moving upward, the upward pulling force was stopped, and the value of the dynamometer was recorded. At the same time, the part was in an approximate equilibrium state. By conducting force analysis on the part, Eq. 17 is expressed as

$$2\mu F + G = F_{\text{pull}} \tag{17}$$

As shown in Eq. 17, gravity G and pulling force F_{pull} can be directly measured by experiments, but another set of experiments is needed to determine the friction coefficient μ between the MR fluid and the workpiece surface. The magnitude of the friction coefficient μ is calculated from experimental data. Figure 7 shows that the part was horizontally placed on the surface of the MR fluid. In order to ensure that the friction coefficient between the part and the MR fluid is the same, a consistent part is required in the measurement process. Due to the light weight of the thin-walled part, there is likely to be errors in the tension value measured in the experiment. Therefore, a piece of aluminum alloy block G_2 with a large mass was put on this part. The dynamometer was used to slowly pull the part along the horizontal direction, and the value F'_{pull} of the dynamometer was recorded when the part was about to move. The force on the part was analyzed with force balance Eq. 18

$$\mu(G + G_2) = F'_{\text{pull}} \tag{18}$$

The fixture was filled with MRF, with the left wall of container as the starting position; the workpieces with different thicknesses were placed in the five positions as shown in Fig. 8 (the attributes, thickness, and position of the workpieces in the container are consistent with Section 2.2).

The container was fixed on the worktable of the machine tool with magnetic field produced by permanent magnets on both sides. The dynamometer was utilized to slowly pull the workpiece along the vertical direction. The average values of the dynamometer in multiple measurements were recorded when the workpiece was about to move.

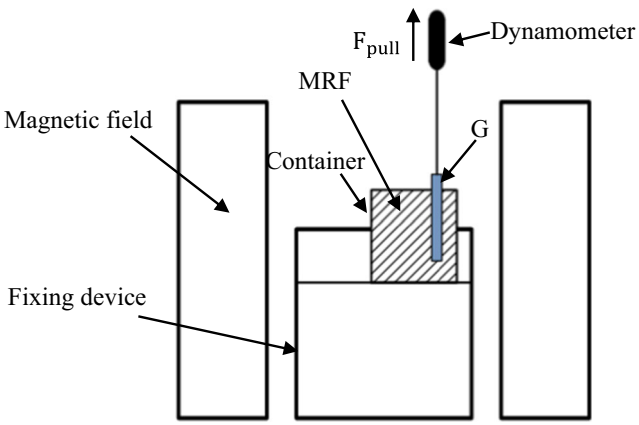

Fig. 6 Schematic diagram of shear stress test

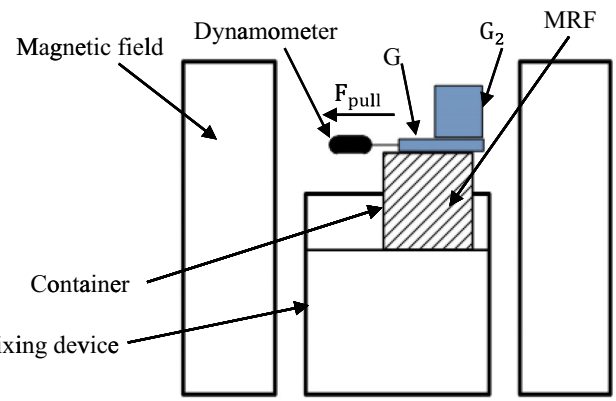

Fig. 7 Schematic diagram of friction coefficient test

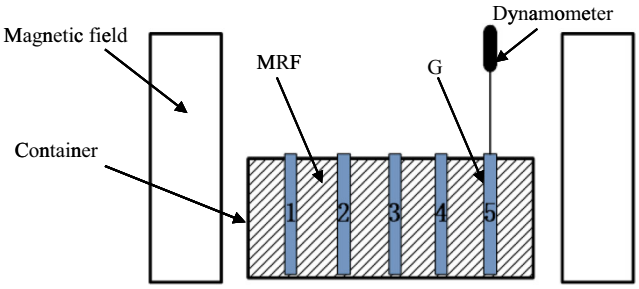

Fig. 8 Schematic diagram of shear stress with experimental measurement

2.4 Experimental processing scheme

In this study, a machining example of milling thin-wall part with rectangular groove was selected to verify the reliability of clamping position of MR flexible fixture in Section 3.2.

Larger diameter tool, lower spindle, larger cutting depth, and higher feed rate are applicable to rough machining with the characteristics of large removal rate. On the contrary, finishing plays a crucial role in ensuring the quality of the parts; choosing the tool with smaller diameter, higher spindle speed, smaller cutting depth, and lower feed rate is necessary. The experimental scheme is as follows: the fixture container is the same as above. The workpieces, which attributes are consistent with Sections 2.2 and 2.3, are aluminum alloy blocks with the size of 50 × 50 × 50 mm. Firstly, clamp the aluminum alloy blank with vise and roughly process it into a rectangular cavity workpiece with a size of 30 × 30 × 30 mm and a wall thickness of 2 mm, then finish it with or without MRF clamping method separately, mill the inner wall of 0.5 mm and then the outer wall of 0.5 mm, with a processing depth of 20 mm, and machine it into a rectangular cavity workpiece with thin-wall of 1 mm. Rough machining experiments were carried out with milling parameters (flat-bottomed cutter ∅10 mm, spindle speed 8000 rpm, cutting depth 2 mm, feed rate 600 mm/min). Furthermore, the workpiece was clamped using MRF and placed at the position in Section 3.2. Finishing cutting experiments were carried out with milling parameters (flat-bottomed cutter ∅3 mm, spindle speed 14,000 rpm, cutting depth 0.25 mm, feed rate 400 mm/min). The cutting force distribution of the two schemes in the machining process was tested using the Kistler dynamometer; the residual stress, flatness, and roughness of the machined parts were respectively measured. Figures 9, 10a, b, 11, and 13 are the diagrams of processing experiment, residual stress test, flatness test, roughness test, and test points. As shown in Fig. 10, TEC4000 was used to test the residual stress of the workpiece in *X*-direction and *Y*-direction. TEC4000 only works in *X*-direction; we are supposed to change the direction of the workpiece when *X*-direction of the workpiece is measured.

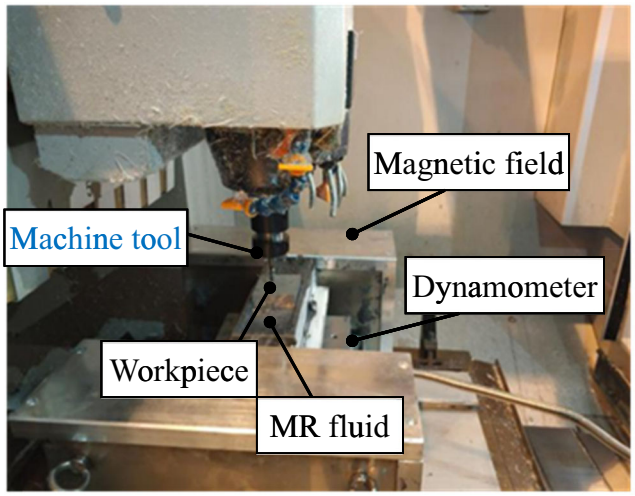

Fig. 9 Diagram of processing experiment

3 Results and discussions

In this section, the relations between magnetic field intensity and the thickness and position of the workpiece were obtained through experiments. The mathematical calculation formula was fitted. Combined with previous theoretical formula, the relations between shear stress and the thickness and position of the workpiece were deduced. Moreover, shear stress experiment was carried out to verify the validity of the theoretical model, and the relations between the true shear stress and the thickness and position of the workpiece were obtained. The optimal clamping position was analyzed based on the theoretical and experimental results. Results demonstrate that the proposed method can effectively improve the surface quality of workpieces.

3.1 Analysis of the relations between magnetic field intensity and the thickness and position of workpiece

In order to obtain the relations between the shear stress and the position and thickness of workpiece, it is necessary to determine the relation between magnetic field intensity and the position and thickness of workpiece. According to the measured experimental data in Fig. 12, it can be seen that the magnetic field intensity on both sides of the workpiece at the same position is different. As the workpiece has magnetic isolation effect, the magnetic field intensity of the far side will decrease with the increase of the thickness of workpiece, and the magnetic field intensity of the near side is greater than that of the far side. As the workpiece is at different positions (Fig. 13), the closer to the magnetic field, the greater the magnetic field intensity of the workpiece, and vice versa. Particularly, at the position of 100 mm far from the container, the magnetic field intensity at the central position of the MR fluid flexible fixture is the smallest. The thinner the workpiece, the smaller the magnetic field intensity on both sides of the middle

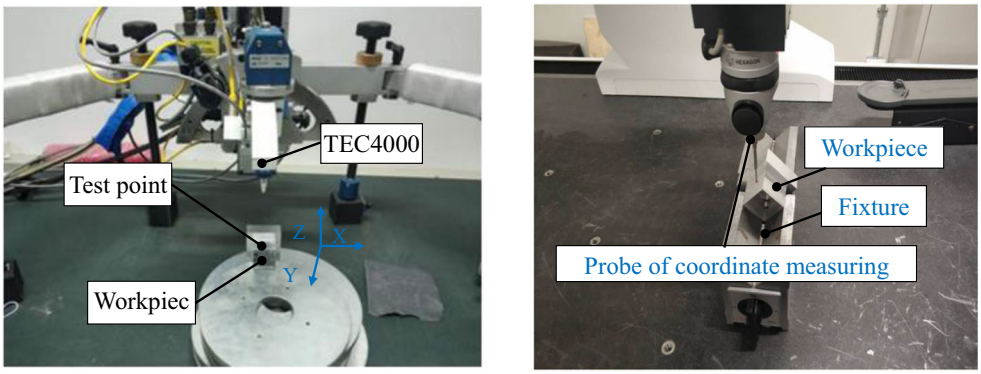

(a) Diagram of residual stress test (b) Diagram of flatness test

Fig. 10 **a** Diagram of residual stress test. **b** Diagram of flatness test

position, and vice versa. At this location, the magnitude of the magnetic field increases with the increase of the thickness of the workpiece.

According to Fig. 12, the approximate mathematical mapping relation between the magnetic field intensity and the thickness and position of the workpiece is fitted

$$H = 39.91 - 0.6602D - 0.2275L + 0.0027D^2 + 0.0060D{\cdot}L - 0.0169L^2 \tag{19}$$

where H is the magnetic field intensity, D is the thickness of workpiece, and L refers to the position of workpiece in the container. By substituting Eq. 19 into Eq. 16, the mathematical relation between the shear stress and the thickness and position of the workpiece is expressed as below:

$$\begin{cases} \tau|_{\gamma=0.37} = 0.9\pi \times 10^{-7} H^2 \sum_{-k_{max}}^{k_{max}} \sum_{-l_{max}}^{l_{max}} \sum_{-n_{max}}^{n_{max}} \dfrac{n(1.144k + 0.37n)\left[4n^2 - (1.144k + 0.37n)^2 - l^2 1.144^2\right]}{\left[(1.144k + 0.37n)^2 + l^2 1.144^2 + n^2\right]^{7/2}} \\ H = 39.91 - 0.6602D - 0.2275L + 0.0027D^2 + 0.0060D{\cdot}L - 0.0169L^2 \end{cases} \tag{20}$$

3.2 Analysis of the relations between experimental and theoretical values of shear stress

In this section, the relations between shear stress and the thickness and position of the workpiece are derived from the experimental data. Meanwhile, the validity of the formula is verified by comparing with the theoretical model obtained in Section 3.1, and the optimal clamping position is obtained. The measured results show that G = 0.21 N, G_2=5.17 N.

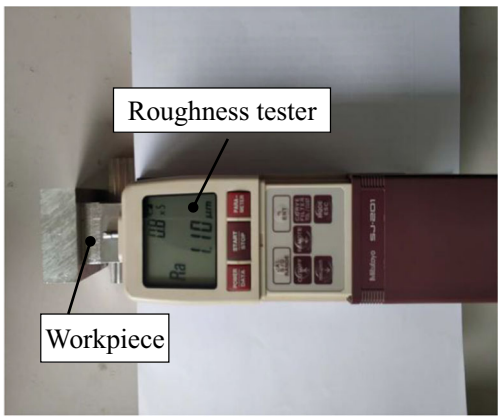

Fig. 11 Diagram of roughness test

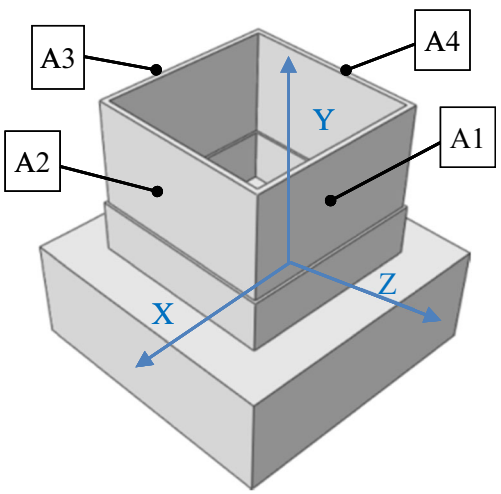

Fig. 13 Diagram of test points

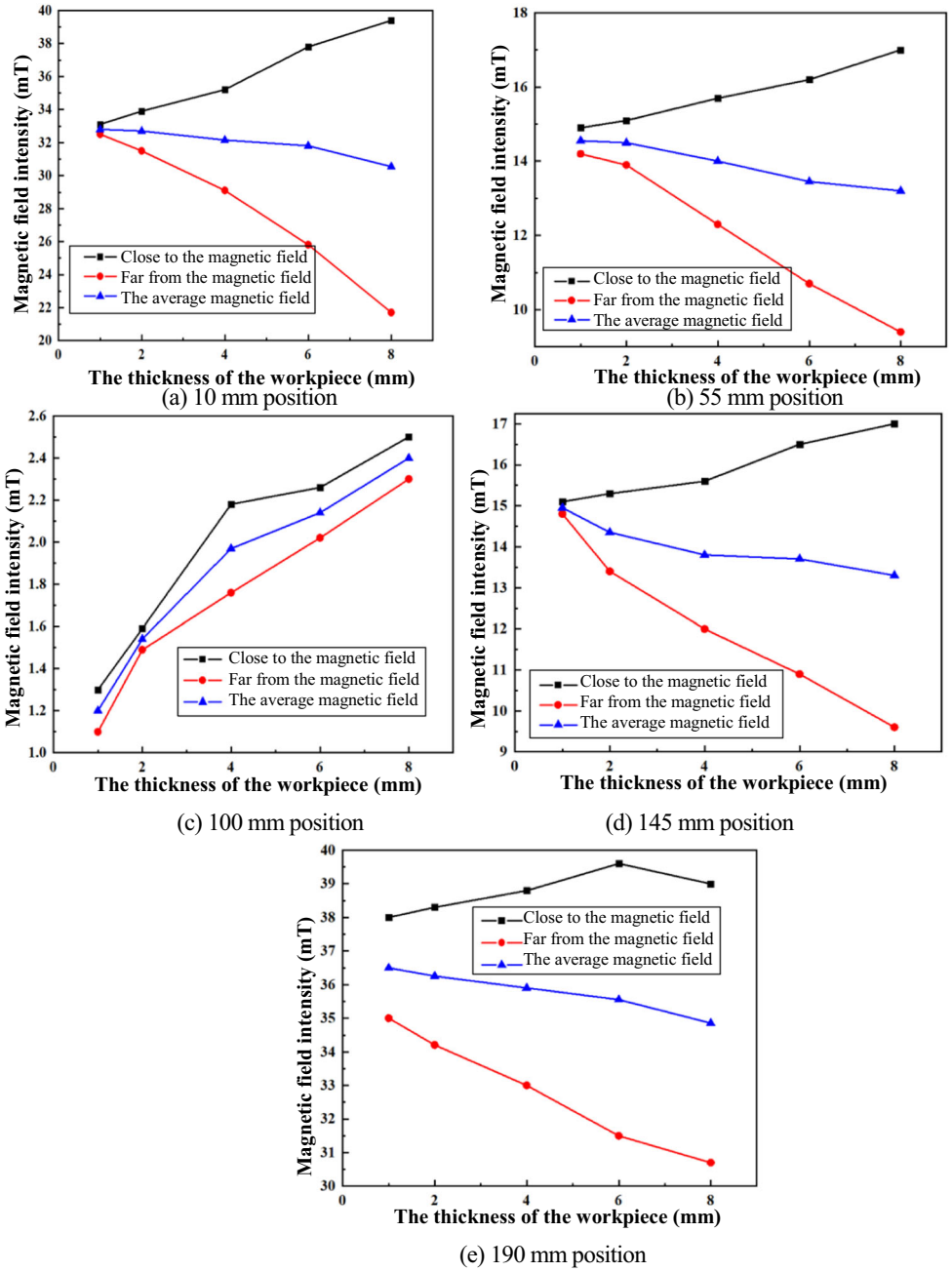

Fig. 12 The relations between magnetic field intensity and the thickness and position of workpiece

Table 1 Actual shear stress values of different thickness and position of the workpiece

Shear stress τ (kPa)		Workpiece position L (mm)				
		10	55	100	145	190
Workpiece thickness D (mm)	1	44.18	6.27	0.35	7.61	44.08
	2	40.37	5.61	0.46	5.12	41.33
	4	39.26	3.67	0.55	4.74	40.61
	6	38.92	3.34	0.62	4.03	40.13
	8	36.36	2.12	0.69	3.55	39.70

After several tests, average value F'_{pull} = 0.11 N, which is substituted into Eq. 14, and $\mu = 0.02$. Finally, μ is substituted into Eq. 19 and Eq. 21 is as follows:

$$F = \frac{F_{\text{pull}} - G}{0.04} \tag{21}$$

Therefore, the shear stress calculation Eq. 22 can be deduced

$$\tau = \frac{F_{\text{pull}} - G}{0.04A} \tag{22}$$

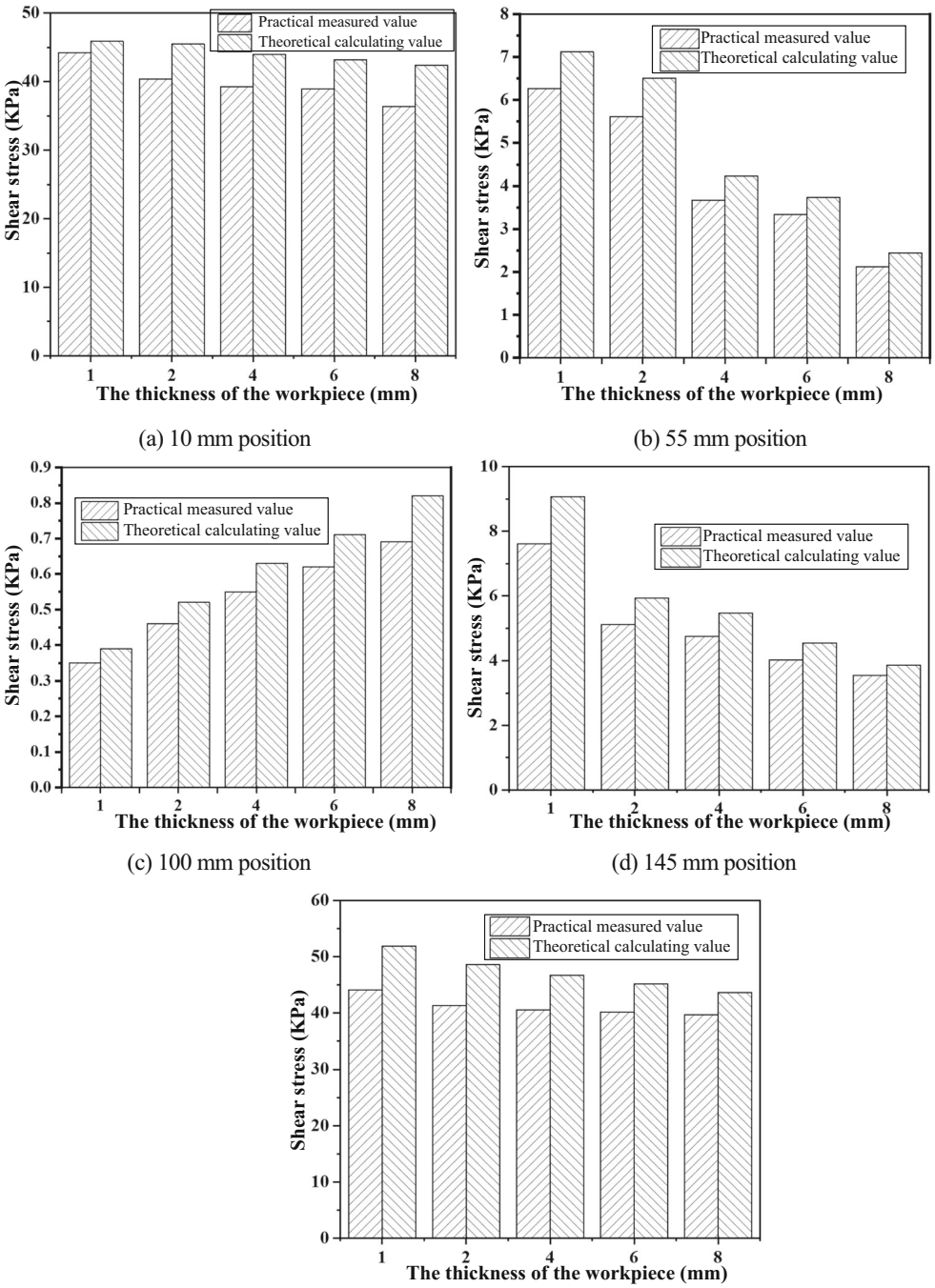

Fig. 14 Numerical comparison of theoretical and true shear stress

As shown in Table 1, the measured values in Section 2.3 are substituted into Eq. 22 to calculate the shear stress values of different thickness and position of the workpiece. As shown in Fig. 14, the thickness and position values of the workpiece in Table 1 are substituted into the Eq. 20 to calculate the theoretical shear stress values, which are compared with the actual shear stress values.

As shown in Fig. 14, the theoretical value is larger than the actual value; the upward and downward trends tend to be consistent. The maximum errors are controlled within 20% by calculating the theoretical values and actual values at the same position and thickness. It can be verified the reliability of Eq. 20 in calculating the shear stress of the workpieces with different thicknesses at different positions. The actual shear stress value is drawn in Fig. 15 to reflect the relations. As can be seen from Fig. 15, except for the middle location, the workpieces with different thicknesses have different shear stress values at the same position, and the shear stress

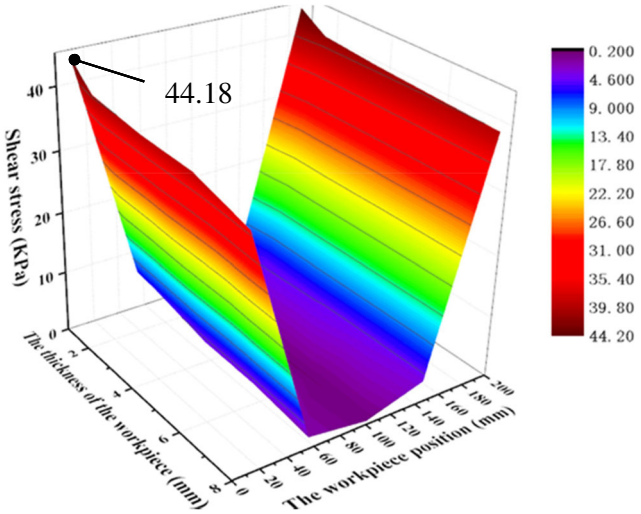

Fig. 15 The relations between the thickness and position of the workpiece and the shear stress

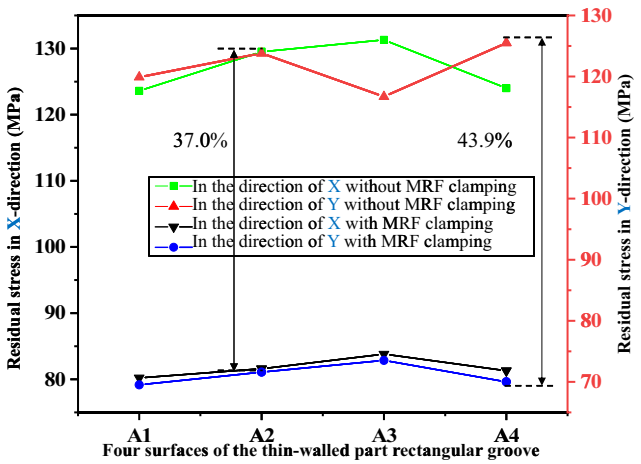

Fig. 16 Tests of residual stress of thin-walled part rectangular groove

decreases with the increase of the thickness. The shear stress on the workpieces with different thickness reaches the minimum value in the middle location, and the shear stress increases with the increase of thickness. The largest shear stress of the workpiece 1 mm thick is 44.18 kPa at the position of 10 mm. The shear stress of the part with the same thickness tends to be u-shaped and varies at different positions. The largest shear stress appears at both ends, while the shear stress at the middle position is the smallest. However, the numerical variation of shear stress caused by the change of workpiece thickness is much smaller than that caused by the change of workpiece position. According to the above analysis, the smaller the thickness of the workpiece and the closer to the magnetic field, the greater the magnetic field intensity and the shear stress value, and the better the clamping effect of the MR fluid fixture. Therefore, the thin-walled workpiece should be processed near the magnetic field. Moreover, the smaller the thickness, the better the clamping effect, and the more stable the machining process.

3.3 Analysis of experimental results

In this section, experiments on the processing of rectangular thin-walled part were conducted to verify the conclusion obtained in Section 3.2: the smaller the thickness of the part, the closer to the magnetic field, the greater the shear stress value, and the better the clamping effect will be.

Table 2 shows the cutting force values of two milling schemes for the rectangular thin-walled workpiece. The cutting force values in three directions decrease when using MRF to machine with clamping location in Section 3.2. The maximum cutting force in the *Z*-direction is 14.51 N; the minimum cutting force in the *X*-direction is 4.72 N. The reduction of the cutting force in the *X*-direction is the highest, which is 14.3%. The reduction in the *Z*-direction is the smallest, which is 7.2%. It can be inferred that the machining with the MR fluid flexible fixture can significantly influence the cutting force in the *X*-direction and has the least influence on the cutting force in the *Z*-direction.

Figure 16 and Table 3 show the test values of residual stress and roughness of four surfaces A1, A2, A3, and A4 of the thin-walled part rectangular groove, and the test diagram is shown in Fig. 13. Compared with no MRF clamping, the residual stress and roughness with MRF clamping position in Section 3.2 are significantly improved. The maximum decrease of residual stress σ_x and σ_y is 37.0% and 43.9%, respectively. Compared with A2, A3, and A4 faces, A1 face is closer to the magnetic field, so the machining process is stable with good clamping effect, and the residual stress is slightly lower than the other three faces. The maximum decrease of roughness R_a, R_z, and R_q is 55.6%, 53.2%, and 56.7%. Table 4

Table 2 Cutting force values with or without MRF clamping

Clamping method	F_x maximum cutting force (N)	F_y maximum cutting force (N)	F_z maximum cutting force (N)
Without MRF	5.51	6.47	15.63
With MRF	4.72	5.62	14.51
Decrease (%)	14.3	8.0	7.2

Table 3 Tests of roughness of thin-walled part rectangular groove

Clamping method		A1	A2	A3	A4
Without MRF	R_a (μm)	1.33	1.10	1.04	1.35
	R_z (μm)	6.47	4.76	5.75	6.93
	R_q (μm)	1.58	1.12	1.28	1.64
With MRF	R_a (μm)	0.65	0.61	0.58	0.60
	R_z (μm)	3.25	3.18	3.07	3.24
	R_q (μm)	0.76	0.74	0.68	0.71

Table 4 Planarity of thin-walled rectangular grooves

Clamping method	Surface	+TOL (mm)	MEAS (mm)	DEV (mm)	OUTTOL (mm)
Without MRF	A1	0.010	0.026	0.026	0.016
	A2	0.010	0.023	0.023	0.013
	A3	0.010	0.019	0.019	0.009
	A4	0.010	0.027	0.027	0.017
With MRF	A1	0.010	0.014	0.014	0.004
	A2	0.010	0.013	0.013	0.003
	A3	0.010	0.014	0.014	0.004
	A4	0.010	0.012	0.012	0.002

shows that the flatness values of A1, A2, A3, and A4 on four surfaces of rectangular groove thin-walled workpieces with or without MRF clamping are obtained by flatness testing. As can be seen from the table, the flatness value with MRF decreases by 55.6%.

Based on the above analysis, it can be concluded that the clamping position of the MR fluid flexible fixture in Section 3.2 can greatly improve the surface quality and processing accuracy of the workpiece, which verifies the reliability of the conclusion in Section 3.2.

4 Conclusion

Based on the experiments on magnetic field intensity and part position and thickness, a new theoretical formula for calculating the shear stress of MRF and the position and thickness of workpiece was proposed. By combining the shear stress test of magnetorheological fluid fixture and the mathematical formula, the real value of shear stress corresponding to the thickness and position of the workpiece was calculated, and the real value was compared with the theoretical value. Finally, the accuracy of the proposed method was confirmed by carrying out milling experiments. The conclusions are summarized as follows:

1. In the process of installing and clamping thin-walled parts with magnetorheological fluid, the intensity of the near magnetic field is much higher than that of the far magnetic field at the same position. At different positions, the closer to the magnetic field, the stronger the field. Particularly, the magnetic field on both sides at the middle position of 100 mm is enhanced with the increasing thickness of the workpiece.
2. The theoretical shear stress value is larger than the real value, both of which show the same upward and downward trends. The error is within 20%, which can verify the validity of the proposed theoretical formula. By analyzing the real value, the smaller the thickness, the closer the workpiece to the magnetic field, the greater the shear stress, and the better the clamping effect. Among them, the shear stress of the workpiece 1 mm thick at the position of 10 mm is the maximum, which is 44.18 kPa. Furthermore, thickness has less influence on shear stress than position.
3. The results demonstrate that the cutting force of machining workpiece decreases by 14.3%, the residual stress σ_x and σ_y drops by 37.0% and 43.9%, the flatness value decreases by 55.6%, and the roughness R_a, R_z, and R_q falls by 55.6%, 53.2%, and 56.7%, respectively. The reliability of the above theoretical model and the proposed method is verified.

To sum up, the proposed mathematical model of shear stress and the method for the magnetorheological flexible clamping system apply to optimization analysis of specific engineering applications to obtain the best process scheme. The results provide a new idea for controlling the machining quality of thin-walled parts by using flexible fixture of MRF in various fields such as aerospace and automobile.

Funding information This project is supported by the Innovation Funding of Shanghai Aerospace Science and Technology (Grant No. SAST2019-065) and the Shanghai Science and Technology Commission (Grant No. 19060502300).

References

1. Zhou L, He L, Zheng YJ, Lai X, Ouyang MG, Lu LG (2020) Massive battery pack data compression and reconstruction using a frequency division model in battery management systems. J Energy Storage. https://doi.org/10.1016/j.est.2020.101252
2. Arnaud L, Gonzalo O, Seguy S, Jauregi H, Peigne G (2011) Simulation of low rigidity part machining applied to thin-walled structures. Int J Adv Manuf Technol 54(5-8):479–488
3. Zhou X, Zhang DH, Luo M, Wu BH (2009) Toolpath dependent chatter suppression in multi-axis milling of hollow fan blades with ball-end cutter. Int J Adv Manuf Technol 72(5-8):643–651
4. Cep R, Petru J, Zlamal T, Valicek J, Harnicarova M, Janasek A, Cepova L. (2013) Influence of feed speed on machined surface quality. International Conference On Metallurgy And Materials 1033-1038
5. Dong XF, Zhang WM (2017) Stability analysis in milling of the thin walled part considering multiple variables of manufacturing systems. Int J Adv Manuf Technol 89(1-4):515–527

6. Savadamuthu L, Muthu S, Vivekanandan P (2012) Optimization of cutting parameters for turning process using genetic algorithm. Eur J Sci Res 69(2):73–80
7. Hareendran M, Sreejith S (2018) A study on surface quality of thin-walled machined parts. Mater Today-Proc 5(9):18730–18738
8. Kant G, Sangwan KS. (2015) Predictive Modelling and optimization of machining parameters to minimize surface roughness using artificial neural network coupled with genetic algorithm. 15th Cirp Conference On Modelling of Machining Operations 31:453-458
9. Ding ZS, Sun GX, Guo MX, Jiang XH, Li BZ, Liang SY (2020) Effect of phase transition on micro-grinding-induced residual stress. J Mater Process Technol:281. https://doi.org/10.1016/j.jmatprotec.2020.116647
10. Tandon V, EI-Mounayri H, Kishawy H (2002) NC end milling optimization using evolutionary computation. Int J Mach Tool Manu 42(5):595–605
11. Hauth S, Richterich C, Glasmacher L, Linsen L (2011) Constant cusp tool path generation in configuration space based on offset curves. Int J Adv Manuf Technol 53(1):325–338
12. Rao RV, Pawar PJ (2010) Parameter optimization of a multi-pass milling process using non-traditional optimization algorithms. Appl Soft Comput 10(2):445–456
13. Jiang XH, Li BZ, Yang JG, Wu HL (2011) Research on the properties of milling and the process parameters optimization for aluminum-alloy thin-walled parts. Front Manuf Design Sci 44-47: 2842–2846
14. Jiang XH, Li BZ, Yang JG, Zuo XY (2013) Effects of tool diameters on the residual stress and distortion induced by milling of thin-walled part. Int J Adv Manuf Technol 68(1-4):175–186
15. Jiang XH, Kong XJ, Zhang ZY, Wu ZP, Ding ZS, Guo MX (2020) Modeling the effects of Undeformed Chip Volume (UCV) on residual stresses during the milling of curved thin-walled parts. International Journal of Mechanical Sciences 167. https://doi.org/10.1016/j.ijmecsci.2019.105162
16. Wu CJ, Pang JZ, Li BZ, Liang SY (2019) High-speed grinding of HIP-SiC ceramics on transformation of microscopic features. Int J Adv Manuf Technol 102:1913–1921
17. Xiong CH, Wang MY, Xiong YL (2008) On clamping planning in workpiece–fixture systems. IEEE Transact Auto Sci Eng 5(3):407–419
18. Deng HY, Melkote SN (2006) Determination of minimum clamping forces for dynamically stable fixturing. Int J Mach Tool Manu 46(7-8):847–857
19. Kaya N (2006) Machining fixture locating and clamping position optimization using genetic algorithms. Comput Ind 57(2):112–120
20. Asante JN (2008) A combined contact elasticity and finite element-based model for contact load and pressure distribution calculation in a frictional workpiece-fixture system. Int J Adv Manuf Technol 39(5-6):578–588
21. Ratchev S, Phuah K, Liu S (2007) FEA-based methodology for the prediction of part-fixture behaviour and its applications. J Mater Process Technol 191(1-3):260–264
22. Siebenaler SP, Melkote SN (2006) Prediction of workpiece deformation in a fixture system using the finite element method. Int J Mach Tool Manu 46(1):51–58
23. Qin GH, Zhang WH, Wan M (2006) Analysis and optimal design of fixture clamping sequence. J Manuf Sci Eng-Transact ASME 128(2):482–493
24. Liu SG, Zheng L, Zhang ZH, Li ZZ, Liu DC (2007) Optimization of the number and positions of fixture locators in the peripheral milling of a low-rigidity workpiece. Int J Adv Manuf Technol 33(7-8):668–676
25. Raghu A, Melkote SN (2005) Modeling of workpiece location error due to fixture geometric error and fixture-workpiece compliance. J Manuf Sci Eng-Transact ASME 127(1):75–83
26. Meshreki M, Attia H, Kovecses J (2011) Development of a new model for the varying dynamics of flexible pocket-structures during machining. J Manuf Sci Eng-Transact ASME 133(4). https://doi.org/10.1115/1.4004322
27. Meshreki M, Attia H, Kovecses J (2011) A new analytical formulation for the dynamics of multipocket thin-walled structures considering the fixture constraints. J Manuf Sci Eng-Transact ASME 133(2). https://doi.org/10.1115/1.4003520
28. Meshreki M, Kovecses J, Attia H, Tounsi N (2008) Dynamics modeling and analysis of thin-walled aerospace structures for fixture design in multiaxis milling. J Manuf Sci Eng-Transact ASME 130(3). https://doi.org/10.1115/1.2927444
29. Wan XJ, Xiong CH, Wang XF, Zhang XM, Xiong YL (2010) A machining-feature-driven approach to locating scheme in multi-axis milling. Int J Mach Tool Manu 50(1):42–50
30. Zhang XZ, Gong XL, Zhang PQ, Wang QM (2004) Study on the mechanism of the squeeze-strengthen effect in magnetorheological fluids. J Appl Phys 96(4):2359–2364
31. Choi SB, Hong SR, Sung KG, Sohn JW (2008) Optimal control of structural vibrations using a mixed-mode magnetorheological fluid mount. Int J Mech Sci 50(3):559–568
32. Pour DS, Behbahani S (2016) Semi-active fuzzy control of machine tool chatter vibration using smart MR dampers. Int J Adv Manuf Technol 83(1–4):421–428
33. Zhu YS, Gong XL, Li H, Zhang PQ (2006) Numerical analysis on shear yield stress of magnetorheological fluids. J China Univ Min Technol 35(4):0498